Project Report

The Construction and Simulation of V2G System in Micro-grid

Tailei WANG, Venkata Yoganand KONDA, Sagar Bharadwaj

E-PiCo students

Università degli Studi dell'Aquila

June 2022

Abstract

This project emphasize on Vehicle-to-Grid (V2G) technology. In this project V2G is applied to micro-grid and V2G system is constructed based on a parking lot. The structure is proposed in which bidirectional AC/DC and bidirectional DC/DC converters share one common DC bus, and also the coordination control strategy is given. Simulation and results prove the availability of proposed structure and control strategy. The work is meaningful to the control and operation for micro-grid and V2G.

Keywords: Vehicle-to-grid technology, bidirectional AC-DC converters, bidirectional DC-DC converters, electric vehicles

Contents

1 Introduction

1.1 Vehicle-to-grid technology

The electrical vehicle (EV) has revolutionized the transportation sector as it uses electrochemical batteries as power sources instead of fossil fuel-based gasoline, which helps reduce greenhouse gas emissions. Due to technological advances in electronics and bidirectional power inverters, EV is no longer viewed as just transportation tools, but in addition, could serve as electric storage units for the grid by supplying auxiliary services. The concept of the vehicle to grid (V2G) is no longer a fiction, but rather a reality. The transition to EVs will lead toward a green and sustainable transportation system, especially when refueled from renewables. This emerging interest in EVs has led to an exponential increase of EVs integrated as loads into the grid, which might be troubling for the electric grid, resulting in line overloading alongside voltage and frequency instability.

Vehicle-to-grid technology's objective is to balance the peak demand and peak supply and better integrate fluctuating Renewable Energy Systems into the electric grid. It is based on bidirectional power transfer instead of the classical unidirectional charge of the EV batteries. When parked, an EV or an EV fleet will either absorb electricity or provide energy to the grid. The energy flow either from or to the vehicle is controlled via real-time signals depending on the requirement of the electric system and the EV battery state of charge (SOC) [1].

"V2G" means "vehicle-to-grid", it allows the energy to flow in both directions from the grid to the vehicle and also from vehicle to grid. During the V2G mode, the battery is discharged to the grid or to the load. Whereas in the G2V mode bi-directional converter gets the power from the grid to charge the battery.

Here we model both modes of the bi-directional converter. The bi-directional converter is a typical 6-leg inverter that converts AC to DC and also DC to AC. The converter also includes a DC/DC converter along with AC/DC converter. The DC/DC connects with the DC bus of the battery.

1.2 EV battery

An appropriate battery model is necessary to accurately represent the characteristics of an EV battery. There are three methods to model a battery, which are experimental-based model, electrochemical-based model and electric circuit-based model. For this paper, electric circuit-based model is chosen for its capability to represent the electric characteristic of a battery. Shepherd model is represented by a controlled voltage source in series with an internal resistance as shown in Figure 2 [3].

The circuit parameters can be modified to represent a specific battery type and its discharge characteristics. A typical discharge curve consists of 3 sections, see Figure 3.

The first section represents the exponential voltage drop when the battery is charged. The width of the drop depends on the battery type. The second section represents the

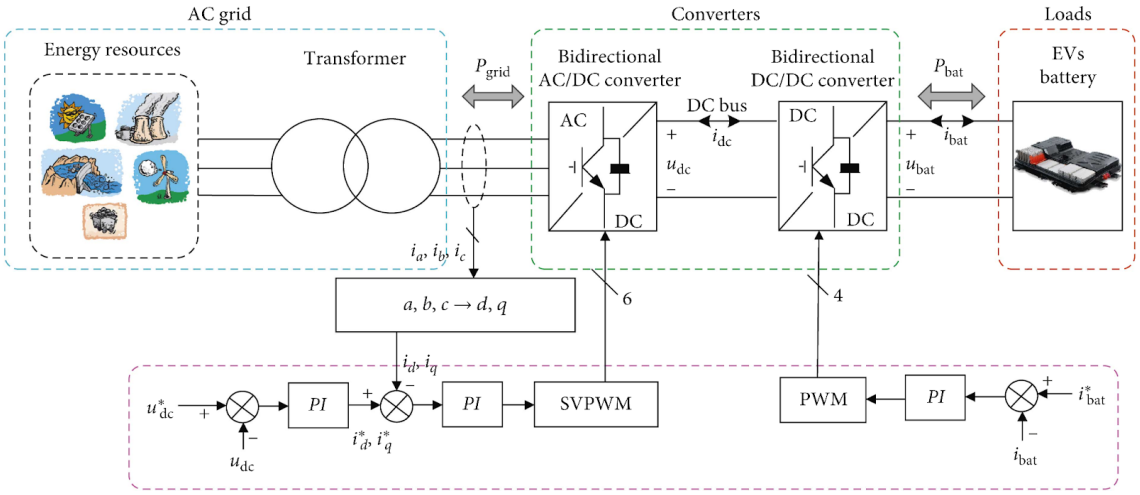

Figure 1: V2G Architecture [2]

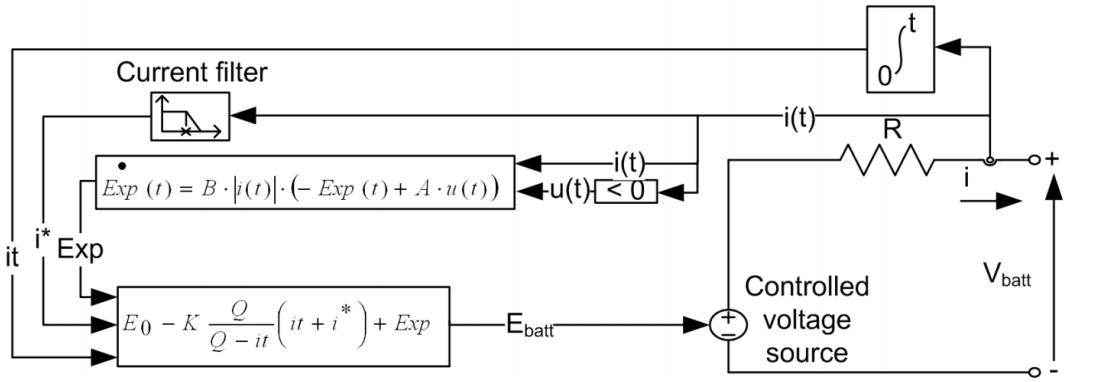

Figure 2: Discharge battery model [4]

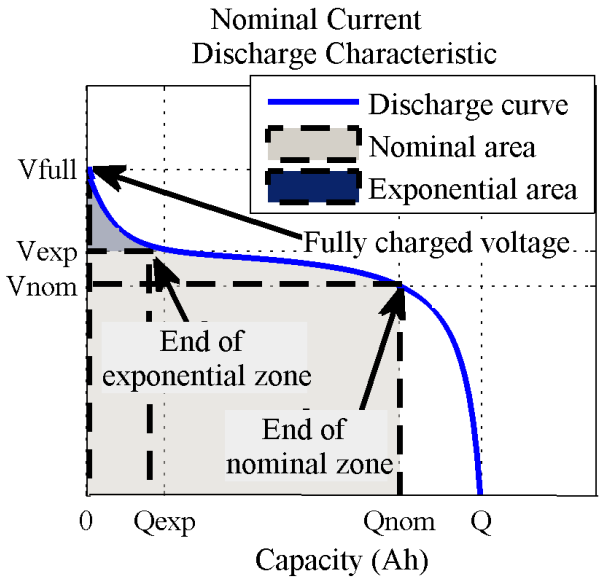

Figure 3: Typical discharge curve [4]

charge that can be extracted from the battery until the voltage drops below the battery nominal voltage. Finally, the third section represents the total discharge of the battery,

when the voltage drops rapidly. The model parameters are derived from the discharge characteristics. The discharging and charging characteristics are assumed to be the same.

For the lithium-ion battery type, the model uses these equations [3].

Discharge Model ($i^\star > 0$)

$$\begin{aligned} &f_1\left(it, i^\star, i, T, T_a\right) = E_0(T) - K(T) \cdot \frac{Q(T_a)}{Q(T_a) - it} \cdot (i^\star + it) + A \cdot \exp(-B \cdot it) - C \cdot it \\ &V_{batt}(T) = f_1\left(it, i^\star, i, T, T_a\right) - R(T) \cdot i \end{aligned} \tag{1}$$

Charge Model ($i^\star < 0$)

$$\begin{aligned} &f_1\left(it, i^\star, i, T, T_a\right) \\ &= E_0(T) - K(T) \cdot \frac{Q(T_a)}{it + 0.1 \cdot Q(T_a)} \cdot i^\star - K(T) \cdot \frac{Q(T_a)}{Q(T_a) - it} \cdot it + A \cdot \exp(-B \cdot it) - C \cdot it \\ &V_{batt}(T) = f_1\left(it, i^\star, i, T, T_a\right) - R(T) \cdot i \end{aligned} \tag{2}$$

1.3 Bidirectional DC-DC converter

One of the useful methods apart from transforming lower and higher voltage for in-vehicle applications is also in V2G (vehicle to Grid) and G2V (Grid to Vehicle) power transfer. Often during high power demand hours, vehicle if not in use and having a higher SOC can be used to supply power back to grid. This is also done by the help of bidirectional converter.

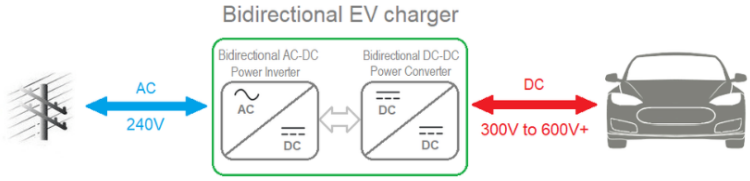

Figure 4: Bidirectional charger

The buck/boost topology is the most basic, see Figure 2.1.1, but because the input and output are not electrically isolated, soft switching is difficult to implement. Non-isolated converters are preferred as the interface between the on-board energy sources when dc conversion ratio is relatively low due to their simple structure, smaller size, and high efficiency.

Additionally, during the turn-on period, the reverse recovery effect of the diode reduces the switching speed of the switch and cannot be neglected in the boost mode. Bidirectional converters are a good alternative for EVs due to their high frequency, power density, efficiency, and dependability.

1.4 Bidirectional three-phase AC-DC converter

Three-phase PWM converters or front-end converters (FECs) are widely implemented for grid-connected electric vehicle chargers (EVCs). VSCs employing pulse width modulation

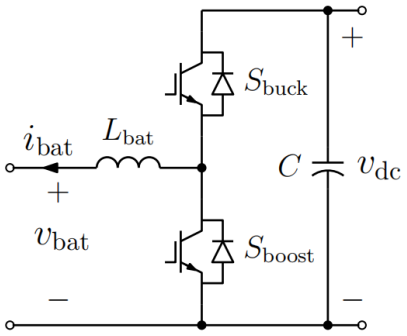

Figure 5: Buck-boost converter [5]

(PWM) techniques are the widest used power converters for applications such as industrial motor drives, robotics, air conditioning and ventilation, uninterruptible power supplies, and electric vehicles. Thus they are also being considered prime candidates for interfacing high-power electronic equipment to power supply lines especially in the case when the load is regenerative.

The topology of a three-phase voltage-source converter is shown in Figure 6. A filter is used to connect to the grid and converter. The ideal AC grid source is denoted as e_a, e_b and e_c. The source currents are i_a, i_b and i_c. L is the inductance filter, and R is the resistance of the series R-L circuit. C is the DC-side capacitor. u_{dc} and i_{dc} are the DC-side voltage and current. A resistance in series is equivalent to the DC load.

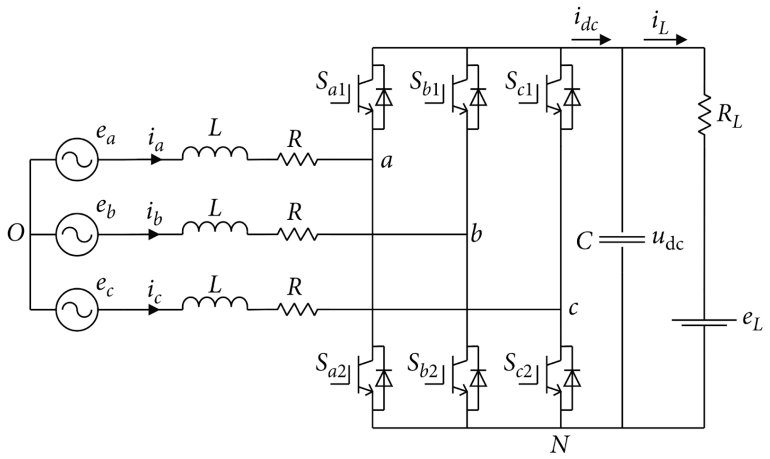

Figure 6: Voltage source converter

In the circuit topology of a three-phase bidirectional voltage source converter (VSC) charger, the charger consists of a battery bank connected to a DC-DC bidirectional converter and a three-phase VSC connected to the power grid. Moreover, the LCL filter is inserted between the inverter and the grid to reduce line current harmonics [6, 7]. The DC-DC converter can operate as a buck or boost converter, depending on the direction of power flow too [5], so the bidirectional VSC charger circuit also enables power transfer from the battery pack to the electricity grid for mostly reactive power support.

1.5 LCL filter

The output current of the inverter connected to the grid contains higher order harmonics because of switching with the pulse width modulation method. Therefore, the L filter is the most commonly used between the inverter and the grid. However, the L filter suppresses existing harmonics. The cost of the L filter is not only very high but also the system dynamic response is slow for large power applications. Besides, a high voltage drop occurs in the L filter [4]. Instead of the advanced L-filter, a high-order LCL filter has been used to correct the output currents of the voltage source converter (VSC) [4, 8]. Passive filters such as the L filter, LC filter, and LCL filters are used for harmonic mitigation in grid-connected inverter systems. The LCL filter effectively smooths the inverter current output, and the filtered harmonic-free current is supplied to the grid. It offers good harmonic elimination with low values of inductors and capacitors.

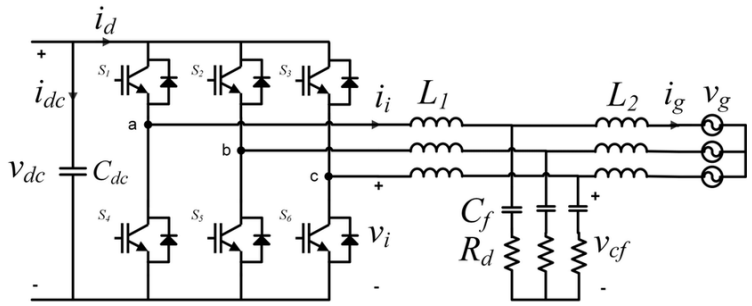

Figure 7: LCL filter

LCL filter design is a bit complex as it starts by taking system parameters such as inverter output voltage, rated active power, grid frequency, switching frequency, and resonance frequency into consideration. The LCL filter has been designed considering that the grid voltage is sensed and the converter current is controlled. LCL filters must be selected according to the current absorbed by the converter. LCL filters are specially designed to reduce harmonics of current absorbed by power converters, with a rectifier input stage. The selection of the inverter side inductance is based on DC voltage, inverter modulation index, switching frequency, and current total harmonic distortion (THD). And the selection of capacitance and grid-side inductance depends on the grid parameters, reactive power, resonance frequency, and ripple attenuation factor RAF [9]. We use the current sensors on the converter side of the filter to get the current information.

In reference [10], the LCL filter parameters are designed by using reactive power ratio and current ripple ratio. If the reactive power ratio and current ripple ratio are not selected properly, they cannot meet the design criteria. As a result, the system is unstable and the LCL filter parameters must be redesigned.

1.6 Phase-locked loop

A system that produces an output signal whose phase is connected to its input is known as a phase-locked loop (also known as a PLL or phase lock loop). The phase difference

between the two signals will either be zero or constant, and they will have the same frequency.

The PLL algorithm can track the phase angle of source voltage vectors for three-phase front-end converters (FECs). They belong to the group of closed-loop synchronization algorithms, which use the feedback of one or more signals in the control structure.

Conventional PLL structures consist of three basic elements: a phase detector (PD) for the signal generation with the phase error information, a loop filter (LF) for phase error elimination, and a frequency/phase generation block also called a voltage-controlled oscillator (VCO).

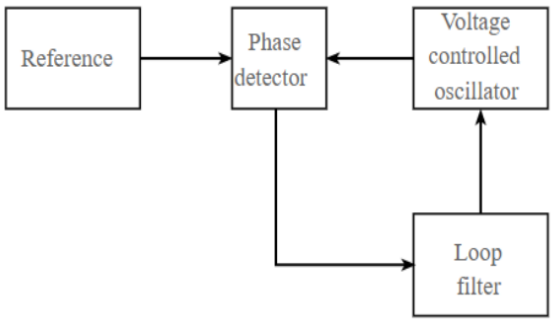

Figure 8: PLL structure

The basic idea of phase locking is to evaluate the difference between phase angle of the input voltage or current signal and generated output voltage or current signal [11]. The phase angle difference between the input signal and output signal is measured by the PD and also provides a proper error signal. To generate the output voltage or current signal, the LF output drives the VCO.

The VCO provides a measure of variations of the phase and generates a signal whose frequency is equal to its input signal [12]. The deviation of the error signal from zero is because of any change in the phase angle (or frequency) of the input signal [13].

2 Control system

2.1 Battery charger control

Before introducing how to control the terminal voltage and the current, it is necessary to discuss two operations of DC-DC converters, which makes it possible for a battery to work in both charging mode and discharging mode.

2.1.1 Buck-Boost Operation of DC-DC converter

As a step-down converter, the Buck DC/DC converter is employed. Step-down refers to the conversion of the input voltage to a lower output voltage. Step-up conversion is

performed using the Boost DC/DC converter. Step-up describes the conversion of the input voltage to a greater output voltage.

The Buck-Boost DC/DC converter may convert the input voltage to either a lower or higher output voltage by acting as both a step-down and step-up converter. The output voltage can be made higher or lower by adjusting the duty cycle.

The generalized diagram of Bidirectional Buck-Boost converter is shown in Figure 2.1.1 with two connected switches and operating in two ON and OFF modes. And this converter can operate in both buck and boost mode.

In buck mode, it is assumed that the converter is working in the continuous conduction, the relationship between the input voltage U_1 and output voltage U_2 is $K_{D1} = U_2/U_1$, where K_{D1} is the duty cycle. The current in the inductor i_L flows from left to right, when $0 \leq t \leq K_{D1}T_s$, Q_1 is on and Q_2 is off, i_L is increasing; when $K_{D1}T_s \leq t \leq T_s$, Q_1 is off and Q_2 is on, i_L is decreasing. The energy from the source V_1 is transferred to the load in V_2 side. The current path in the whole process is shown in Figure 9.

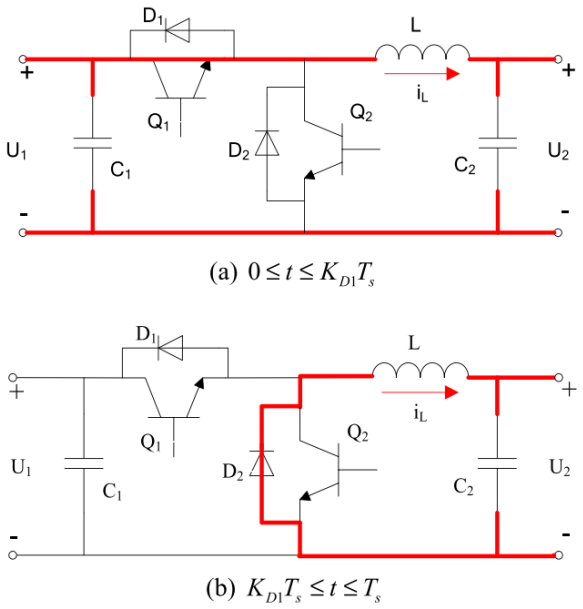

Figure 9: Buck mode [14]

In boost mode, it is assumed that the converter is in continuous conduction too. The relationship between the input voltage U_2 and output voltage U_1 is $U_1/U_2 = 1/(1 - K_{D2})$, where K_{D2} is duty cycle. The current in the inductor i_L flows from right to left, when $0 \leq t \leq K_{D2}T_s$, Q_1 is off and Q_2 is on and i_L is increasing; when $K_{D2}T_s \leq t \leq T_s$, Q_1 is on and Q_2 is off and i_L is decreasing. The energy stored in the inductor together with DC power V_2 supplies to the load in V_1 side. The current path in the whole process is shown in Figure 10.

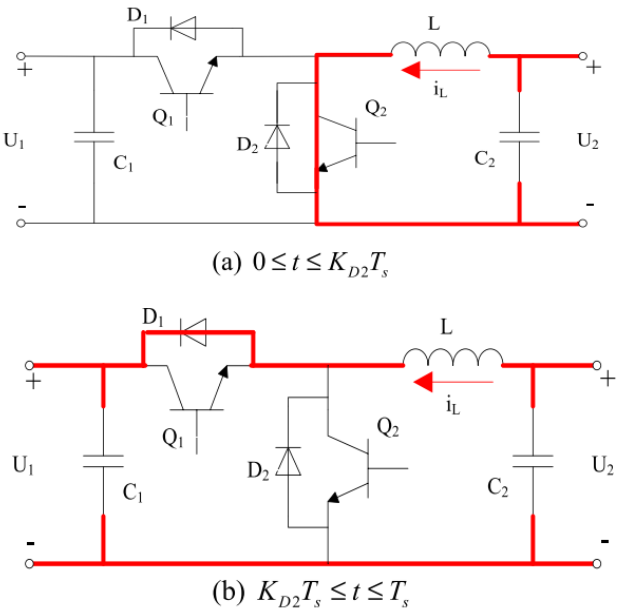

Figure 10: Boost mode [14]

2.1.2 Voltage control with limitations of battery current

The control of DC-DC converter falls into two categories: open-loop control and closed-loop control. For a DC battery charger, its input voltage can be considered as constant. Thus, open-loop control is introduced to control the terminal voltage applying on battery directly by controlling the duty cycle. The relation between terminal voltage U_2 and duty cycle is discussed in Section 2.1.1.

As to closed-loop control, two control methodologies can be implemented depending on desired charging strategy: constant current and constant voltage.

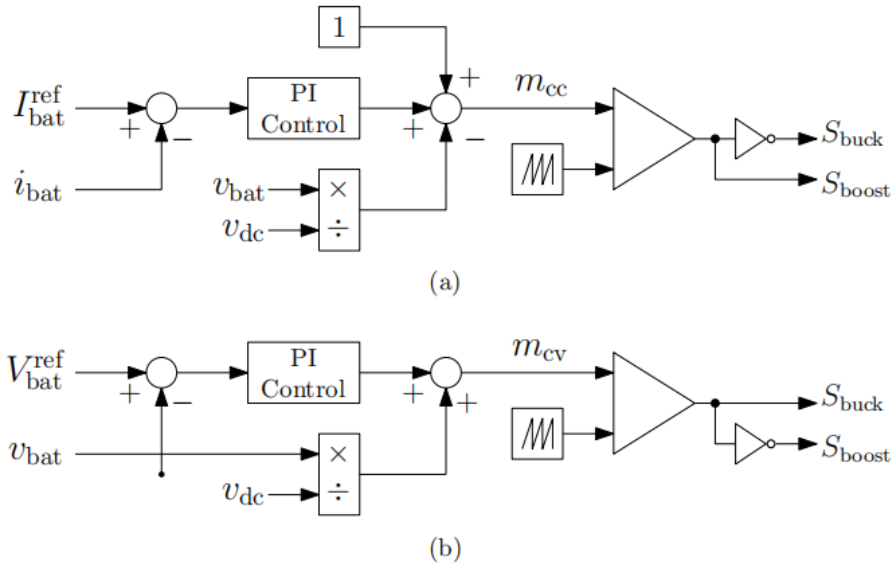

Figure 11: (a) constant current strategy, (b) constant voltage strategy [5]

In practice, it is preferable to control the terminal voltage of battery to be constant. However, the control strategy in Figure 11(b) does not take the limitations of current into account. The current should not be greater than the nominal fast charging value, or it will lead to overheating, shorter battery life and even battery damage.

Therefore, a new control strategy is considered. The idea is to adjust the terminal voltage reference in the voltage controller of battery charger. When the current exceeds the tolerant value, the voltage reference will decrease correspondingly. In this way, the partial voltage across the equivalent resistance of the battery is then reduced, and the current will decrease eventually. The control diagram and further explanation will be demonstrated in Section 3.2.2.

2.2 AC-DC converter control

2.2.1 Clark-Park transform

Three-phase PWM converters include three source voltage (or line current) vectors, separated by 120° from each other, in the phase domain. The phase voltages are defined as:

$$\begin{aligned} V_a &= V_m \cos(\theta_e) \\ V_b &= V_m \cos(\theta_e - 120°) \\ V_c &= V_m \cos(\theta_e - 240°) \end{aligned} \tag{3}$$

where $\theta_e = \omega_e t + \phi$ can be defined and V_m is the amplitude of the phase voltages, ω_e is the angular frequency, ϕ is the phase angle for the three-phase system. The transformation from the three-phase system (a-b-c) to the stationary two-phase system (q_s-d_s) can be illustrated using voltage equations for a three-phase PWM rectifier. Three-phase voltage equations for the front-end converter are given below.

$$\begin{aligned} V_a &= Ri_a + L\tfrac{di_a}{dt} + V_{ia} \\ V_b &= Ri_b + L\tfrac{di_b}{dt} + V_{ib} \\ V_c &= Ri_c + L\tfrac{di_c}{dt} + V_{ic} \end{aligned} \tag{4}$$

where V_{ia}, V_{ib} and V_{ic} are three-phase leg voltages of the converter; i_a, i_b, and i_c are line currents corresponding to phase a, b, and c respectively. R is line resistance and L is line inductance per phase as well.

The voltage equations of the converter in a two-phase stationary reference frame (q_s-d_s) are given below as well.

$$\begin{aligned} V_{sqs} &= Ri_{qs} + L\tfrac{di_{qs}}{dt} + V_{iqs} \\ V_{sds} &= Ri_{ds} + L\tfrac{di_{ds}}{dt} + V_{ids} \end{aligned} \tag{5}$$

where i_{qs} and i_{ds} are current components of the converter; V_{iqs} and V_{ids} are leg voltages corresponding to "q_s" and "d_s" axis respectively.

To obtain the voltage equations of the converter in a two-phase rotating reference frame (q_e-d_e), the equations for the stationary reference frame (q_s-d_s) given in the above

equations are multiplied by $e^{-j\theta e}$. Making some arrangements, the voltage equations in the two-phase rotating reference frame are given below.

$$\begin{aligned} V_{sqe} &= Ri_{qe} + L\frac{di_{qe}}{dt} + \omega_e L i_{de} + V_{iqe} \\ V_{sde} &= Ri_{de} + L\frac{di_{de}}{dt} - \omega_e L i_{qe} + V_{ide} \end{aligned} \tag{6}$$

i_{qe} and i_{de} are current components of the converter; V_{iqe} and V_{ide} are leg voltages corresponding to "q_e" and "d_e" axis respectively [15, 16].

2.2.2 Phase-locked loop

One of the simplest PLL algorithms is SRF-PLL (Stationary reference frame) illustrated in Figure 12. It uses Clarke's and Park's transformation to transfer a three-phase grid voltage vector from *abc* to *dq* frame.

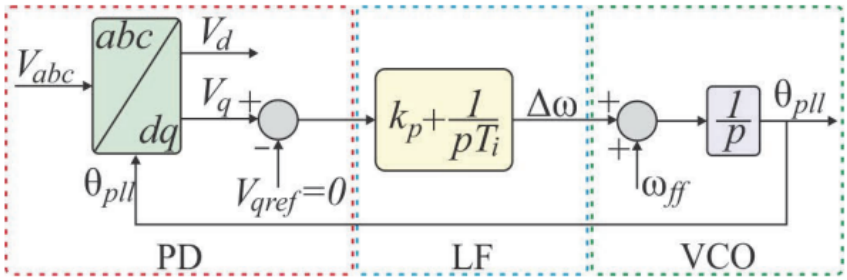

Figure 12: SRF-PLL algorithm

Denote the angle between the grid voltage vector and α-axis as θ. Using trigonometric identities, the direct transformation from *abc* to *dq* frame can be derived as:

$$\begin{bmatrix} v_d \\ v_q \\ 0 \end{bmatrix} = \begin{bmatrix} \cos(\omega t - \theta) \\ \sin(\omega t - \theta) \\ 0 \end{bmatrix} V_m \tag{7}$$

With SRF-PLL angular position of *dq* rotating frame is controlled by the feedback loop. For small angle differences (between ωt and θ), a term $V_m \sin(\omega t - \theta)$ can be approximated as $V_m(\omega t - \theta)$. In the case of the ideal grid voltage vector alignment with the *d* component, the *q* component of grid voltage is zero. The bandwidth of SRF-PLL's control loop can be high, yielding a fast and precise grid phase angle detection, if grid voltage is without either unbalance or harmonics [17]. In case of distorted grid voltage with higher-order harmonics, the bandwidth of the control loop has to be reduced. The most commonly used LF is the PI controller, and since it behaves as a first-order low-pass filter, it does not represent an effective solution for disturbance rejection of dominant higher harmonics in a low voltage grid [18].

2.2.3 Current controller and voltage controller

A cascade control in the *dq*-frame is proposed. It consists of outer voltage loop and inner current loop. Synchronization with the grid voltage is performed through a phase

locked loop (PLL). The proposed control methodology is depicted in Figure 13. The d-axis outer loop controls the DC bus voltage, and the inner loop controls the active AC current. Because the inverter allows bidirectional power flow, increments in the DC bus voltage can be produced from negative or positive current direction and vice versa. In the q-axis, reactive current is controlled by the inner current loop. Additionally, dq decoupling-terms $\omega(L + L_g)$ and feed-forward voltage signals are added to improve the performance during transients.

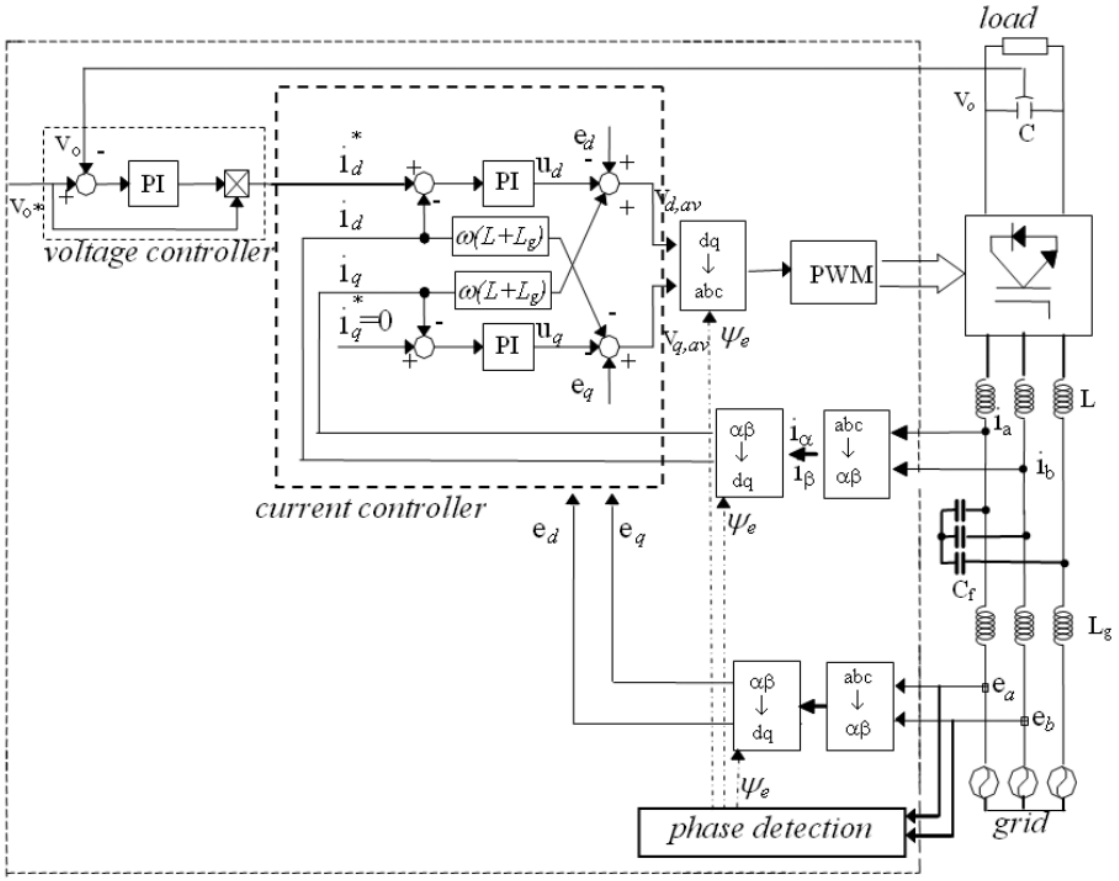

Figure 13: dq-axis oriented cascade control [10]

2.3 Modeling of LCL filter

The output from the converter is not a pure sine wave. Therefore LCL Filter is modeled in order to reduce the current harmonics during the injunction of power to the grid.

Since the grid is assumed to be an ideal voltage source, the transfer function of the LCL filter is

$$\left.\frac{i_g(s)}{U_i(s)}\right|_{U_g(s)=0} = \frac{1}{(L_1 L_2 C_f)\, s^3 + (L_1 + L_2)\, s} \tag{8}$$

Then one can draw its bode diagram as Figure 15. It shows a characteristic of low-pass filter, which is able to reduce high-oder harmonics. However, it also reflects a natural

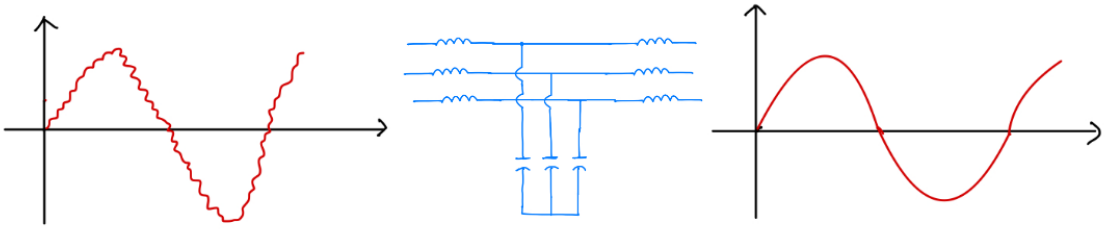

Figure 14: Input harmonics are removed by using a LCL filter

resonance, which means that, at this frequency, the impedance is zero and the current tends to be infinite. In practice, the current cannot become infinite, but may be high enough to damage the system. Consequently, the system must be damped in order to avoid the impedance from being zero at this frequency.

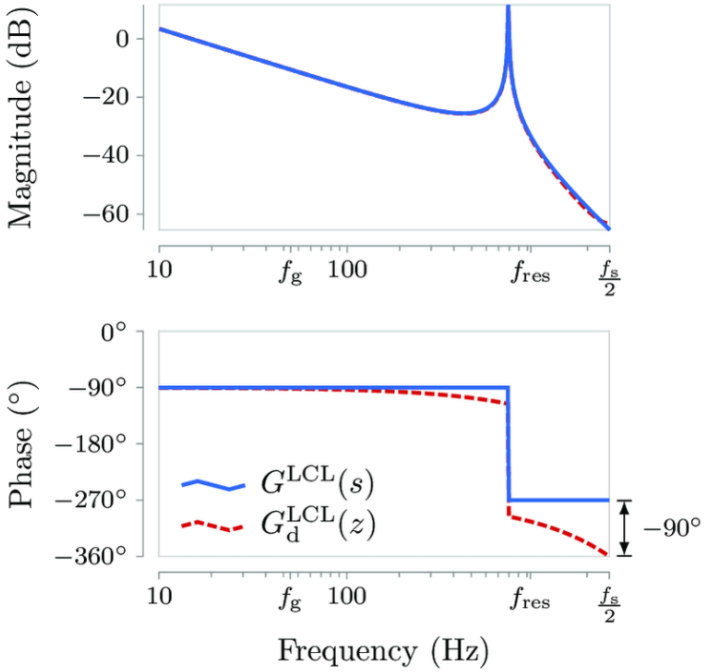

Figure 15: Bode diagram of LCL filters

3 Simulation and results

3.1 Parameter design and calculations

Parameters needed for simulation are introduced or designed in this section. The results are listed in Table 1. The values of E_n and f_b are referred to SAE J1772 standard, and the value of V_o is taken from [5].

The specifications of battery C_{nom} and V_{nom} are taken from the lithium-ion battery used in Tesla Model X Performance [19]. The initial state of charge is set to 50%,

Table 1: V2G system parameters

Parameter	Value	Explanation
E_n	450V	line to line *rms* voltage
f_b	50Hz	grid frequency
C_{nom}	285Ah	battery nominal capacity
V_{nom}	350V	battery nominal voltage
SOC_0	50%	initial state of charge
$I_{MAX,batt}$	100A	the absolute value of maximum battery current
P_n	4.5kW	rated active power
Z_b	45Ω	base impedance
V_o	1.5kV	output voltage of AC-AC converter
ΔV_o	100V	acceptable DC voltage drop
ΔP_{LMAX}	3kW	maximum power excursion
f_{sw}	5kHz	switching frequency of the converters
T_r	2ms	the delays introduced by filtering and control
L	3mH	inductance of the converter side reactor
C_f	1.5μF	capacitance of the LCL filter
L_g	5mH	inductance of the grid side reactor

this value is chosen to ensure that the battery is able to receive or supply power when necessary. Considering in reference [20], the nominal voltage of lithium-ion battery (330V) is close to the one we choose (350V), we assign the same maximum charging current $I_{MAX,batt}$. And what follows is calculation of the values of passive components in V2G system.

The whole design and calculation procedure is instructed by [10].

According to the nominal current discharge characteristic, the maximum battery voltage can be 400V. So in this case the maximum power absorbed from the grid is 40kW. And considering the charging/ discharging efficiency is not exactly 100%, the maximum active power is assigned as 45kW; similarly, the rated active power P_n is designed as 4.5kW. Thus, base impedance can be obtained by:

$$Z_b = \frac{(E_n)^2}{P_n} \tag{9}$$

Under the assumption of a dc voltage level of 1.5kV (V_o) with a maximum acceptable dc voltage drop of 100 V and a maximum power excursion of 3 kW (2/3 rated power assumed design constraint), and considering a delay T_r equal to 2ms, 20μF is enough for a DC capacitor according to

$$C \geq \frac{T_r \Delta P_{LMAX}}{2 V_o \Delta V_o} \tag{10}$$

So here we choose dc capacitance as 200μF in order to guarantee a high ride-through protection capability.

The LCL-filter has been designed considering that the grid voltage is sensed and the converter current is controlled, i.e. the system is as shown in Figure 16.

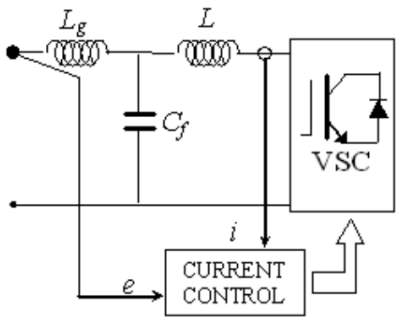

Figure 16: LCL filter with voltage sensed on the grid side and current sensed on the converter side

This choice is justified by the fact that usually in the power range kW–MW in which these converters are used, the current sensors are integrated in the converter and the filter is not integrated (so it is preferable that the current sensors are on the converter side of the filter). Moreover, the over-current protection is also more effective if the current sensors are on the converter side.

Thus the capacitor should be chosen equal to the lower in respect to L_g/Z_b^2 or to L/Z_b^2. A value of $L = 3$ mH is enough to limit the switching ripple on the converter side and not to saturate the inductors.

Then, it has been chosen to have $L < L_g$ and $C_f = L/Z_b^2$ and to use the value of L_g to tune the LCL-filter. The choice has the inherent advantage to have a resonance frequency of the system less dependent on the grid side inductance. Thus the capacitor value has been chosen equal to 1.5μF. The grid side inductance has been chosen to have 10% of the switching ripple of the converter side, according to (11), thus $L_g = 5$mH.

$$\frac{i_g}{i} \approx \frac{1}{\left[(1+r) - r\left(f_{sw}/c\right)^2\right]} \tag{11}$$

where $r = L_g/L$ and $c = Z_b/(2\pi L)$.

3.2 Simulation results

In this section, in order to ensure a better performance of the whole V2G system, battery charger and AC-DC converter are simulated and tested separately. The role of control system is demonstrated and discussed as well.

3.2.1 Battery characteristic curve

The battery model in our simulation is the built-in model in the Simulink library. Given the nominal parameters in Section 3.1, it determines other parameters and coefficients of non-linear characteristics based on Shepherd model [3], such as internal resistance, fully charged voltage, coefficients in the exponential zone, etc. The internal temperature T

and environment temperature T_a in (1) and (2) are set to be constant by default, which means corresponding coefficients are constant as well.

After assigning the nominal parameters, discharge characteristic curves can be obtained as shown in Figure 17.

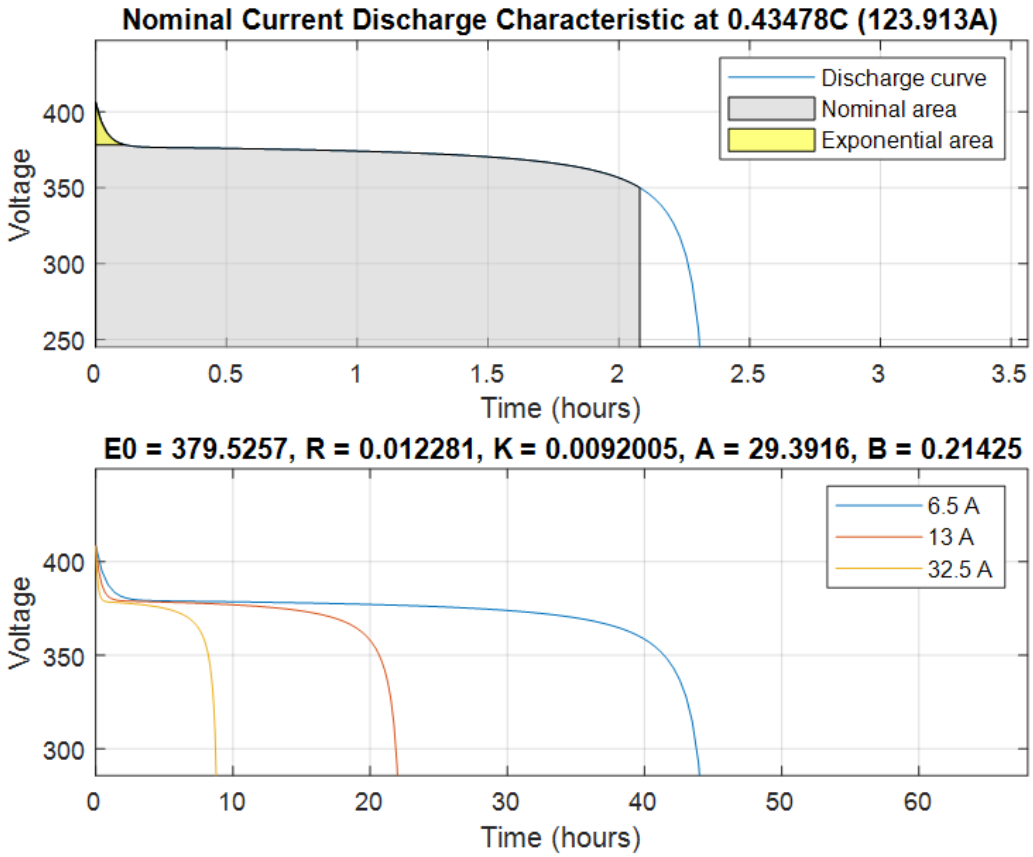

Figure 17: Discharge characteristic curves of the assigned model

It can be observed that in our case nominal area counts for the vast majority, which is reasonable. And the greater the given current, the faster the terminal voltage of the battery drops.

3.2.2 Battery charger simulation

The general Simulink model of battery charger, i.e. a battery, a constant DC voltage source plus a DC-DC converter, is shown as Figure 18.

The topology is the same as schematic diagram shown in Figure 5. It should be noted that `UG` and `LG` are PWM control signals of the upper and the lower MOSFETs respectively. Both signals are outputs from battery controller as Figure 19 shown.

It can be seen that the control strategy is based on an open-loop control of duty cycle by setting a constant voltage reference of the left port of DC-DC converter, i.e. the terminal voltage of battery. If the voltage reference is set to be greater than battery

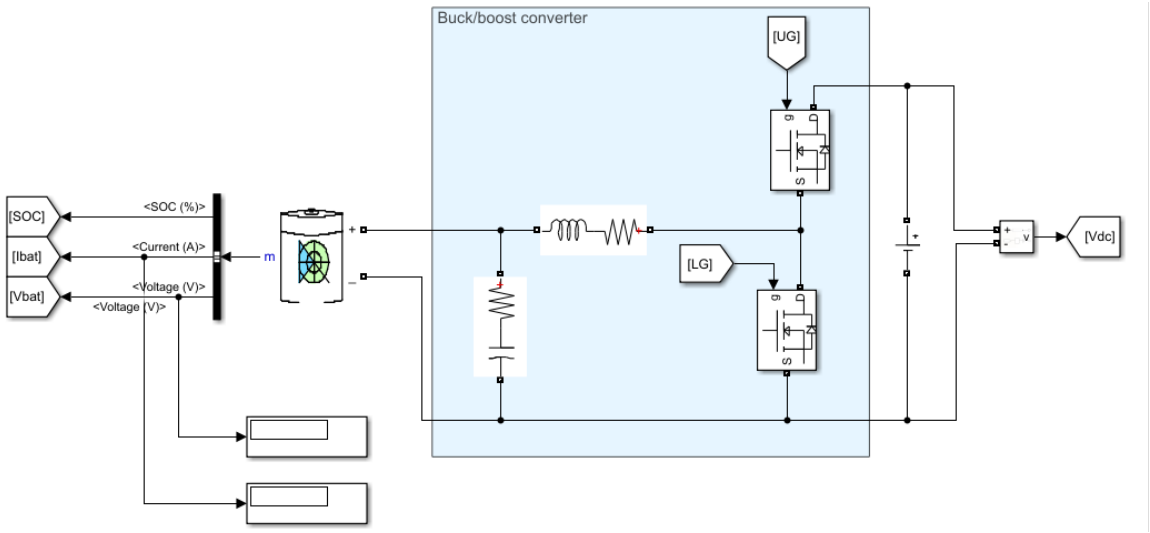

Figure 18: Battery charger simulation

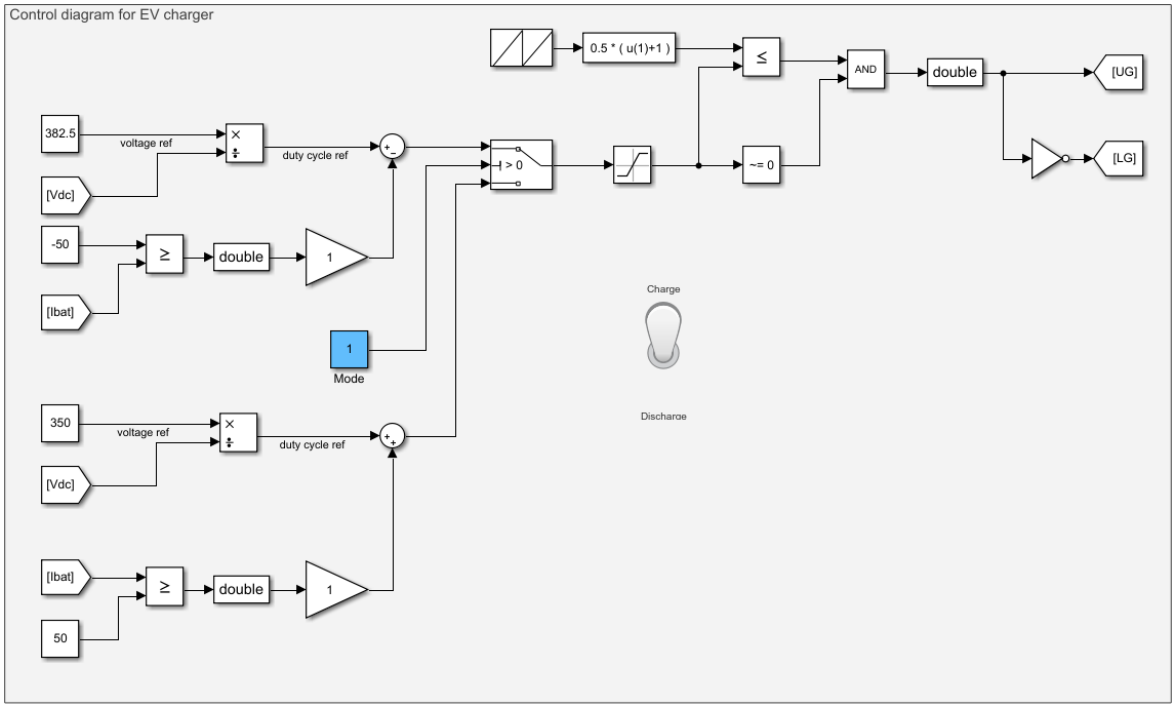

Figure 19: Battery charger controller

voltage, then the battery is in charging mode, and the value of current is negative; conversely if the voltage reference is less than battery voltage, the discharging current values in positive.

However, if the charger is simply controlled in such an open loop, the battery will face a problem that the current goes above maximum battery current $I_{MAX,batt}$. As shown in Figure 20.

Figure 20 shows the simulation result when one just using an open-loop voltage control for the battery charger. The voltage reference is set to be 382.5A, which is the maximum

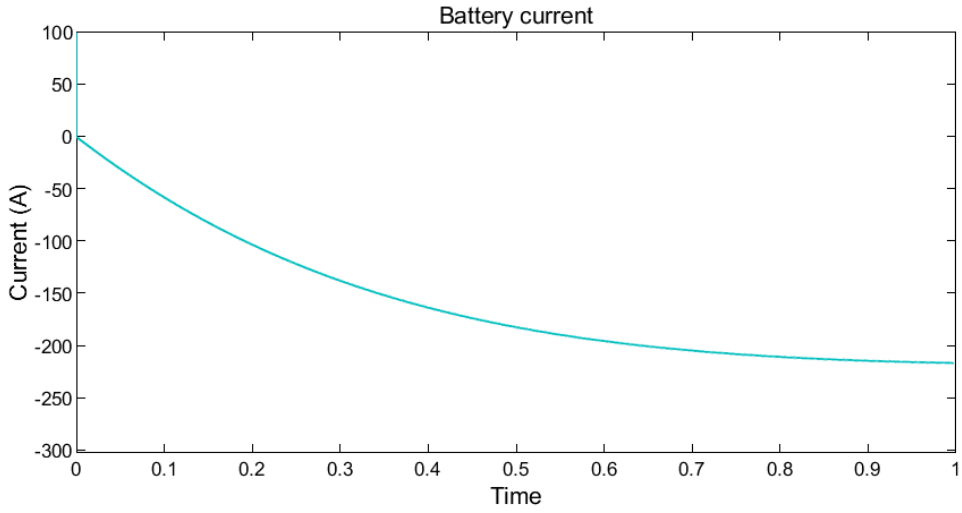

Figure 20: Current exceeds maximum charging current

voltage in nominal area of the charge/ discharge characteristic in Figure 17. One can see that the charging current has already exceeded $I_{MAX,batt}$ in less than 0.5s.

This phenomenon can be solved by limiting the value of battery current. We introduced an approach which can adjust the control signal by taking the limitation of current into account, as shown in Figure 19. The limitation of current is set to be $\pm$50A.

By introducing a negative feedback regarding charging/ discharging current, the battery controller is in sliding mode: When the amplitude of current is below 50A, the control signal is effected by voltage reference only, thus the duty cycle reference is a positive constant value; while it exceeds 50A, the duty cycle reference is modified to reduce a certain constant value, in our case we simply set it to 1. After the saturation block (which lower bound is 0), the duty cycle reference is 0.

In other words, suppose when the battery is charging, only when the current is under the limitation, DC-DC converter is in buck mode (Figure 9); otherwise the lower MOSFET is on and the upper one is off during that instant no matter the time is in high level moment or not. In this way, the battery voltage will decrease to eliminate the over-current.

Therefore, we can obtained the charging curves under the new control law, see Figure 21. It can be seen that current is controlled to be under the limitation of $-$50A. And also the voltage is controlled to be constant. One can observed that there is an instant step of both voltage curve and current curve at the beginning of simulation. This is because the initial voltage of battery is much less than the reference output voltage of DC-DC converter.

The function of limiting current is demonstrated in Figure 22 and Figure 23. Since the duty cycle is measured from the control signal of lower MOSFET, the duty cycle of the DC-DC converter is "$-$`DutyCycle`" in the figures.

One can see that when the current start to chatter around $-$50A, the duty cycle increases from 25.3% to 24.8%. This is because when the current is above its limitation,

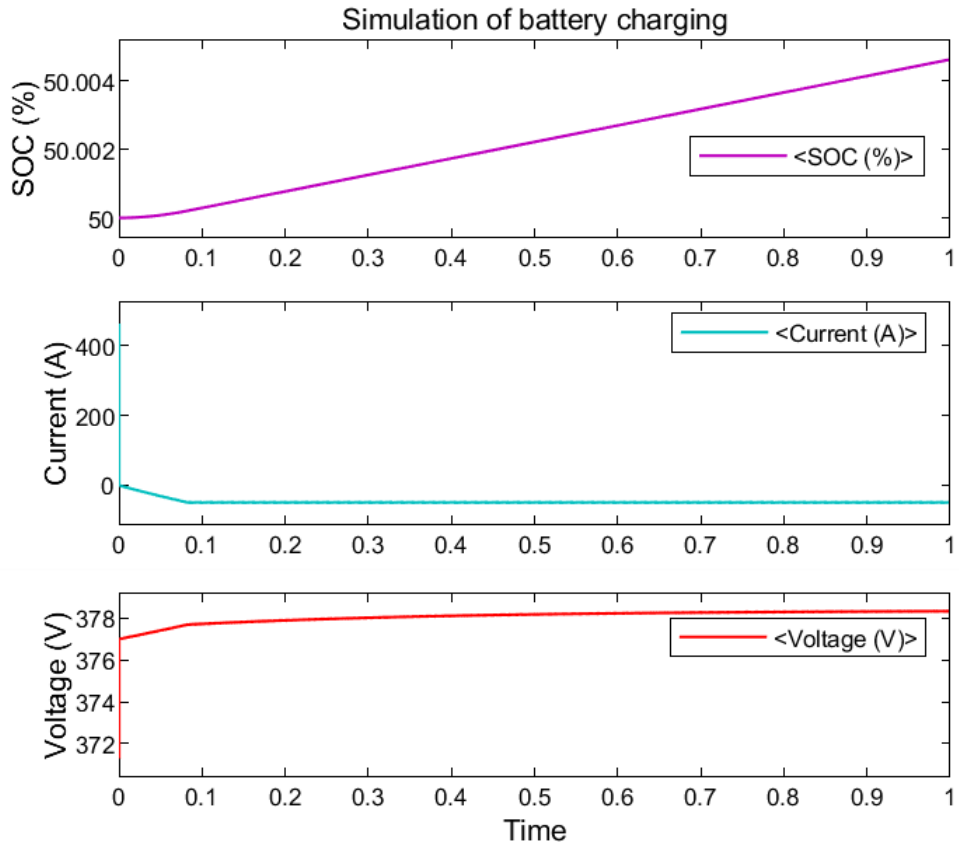

Figure 21: The simulation of battery charging under the controller

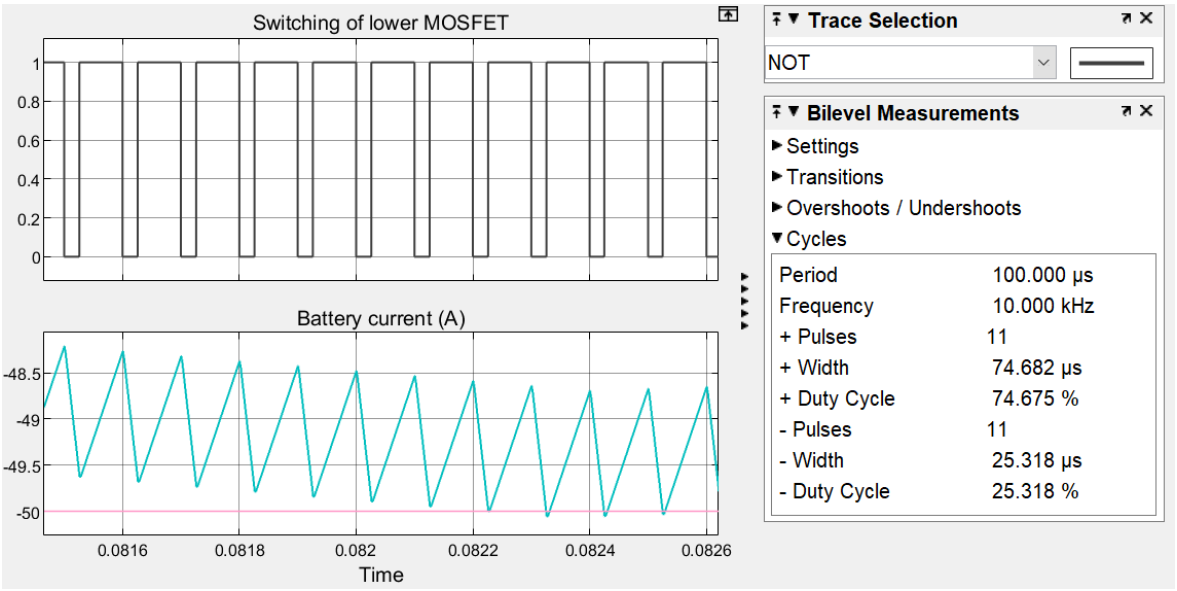

Figure 22: The switching of the lower MOSFET when current is above -50A

the lower MOSFET is always on and upper one is always off. In this way the voltage reference will decrease correspondingly to reduce the current.

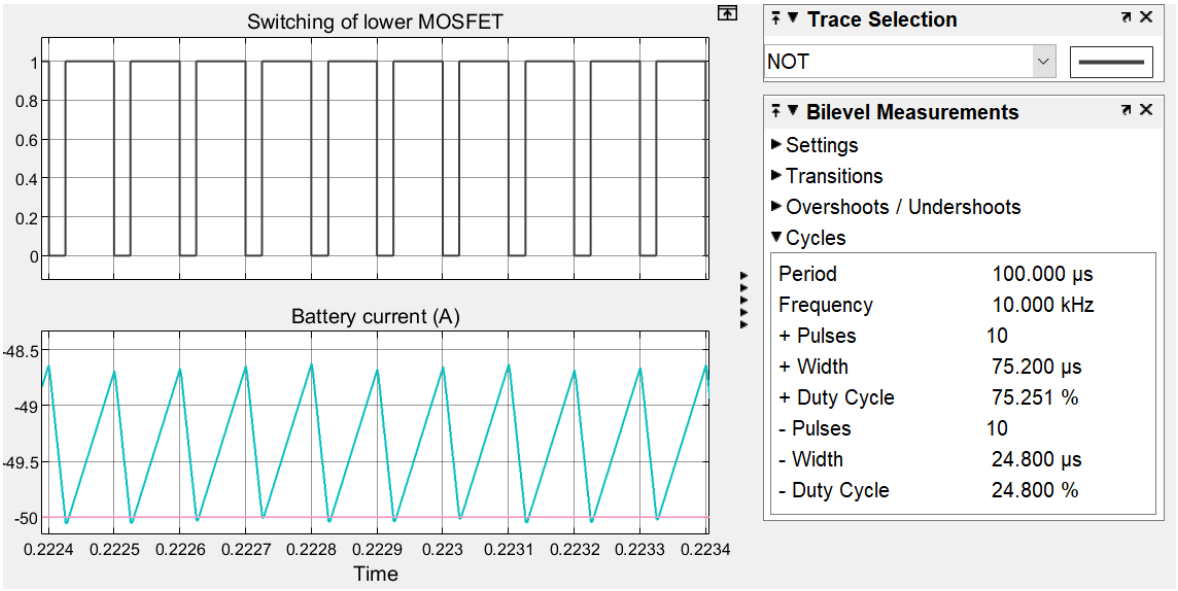

Figure 23: The switching of the lower MOSFET when current is below -50A

The `mode` block in Figure 19 controls the battery charge or discharge. Since the control strategy is similar when the battery is discharging, the discharging curves are not demonstrated here, which will be shown in Section 3.2.5.

3.2.3 LCL filter test

LCL filter is modeled in the Simulink and tested before we connect it connected to the VSC, see Figure 24.

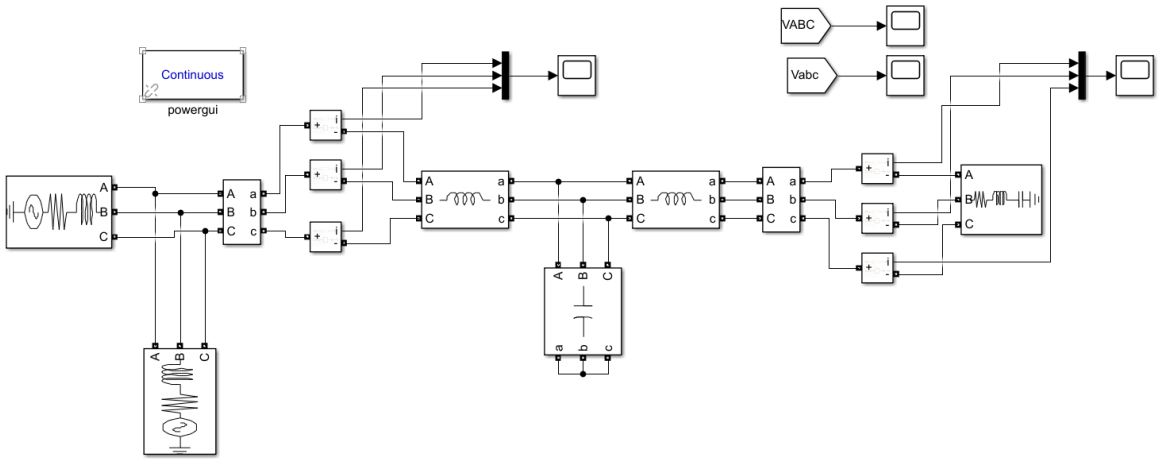

Figure 24: The simulation of the LCL filter

A 3-phase power source is used as a grid, additional noise is generated in the grid by introducing voltage disturbance. The inductance and capacitor values were chosen in such a way as to minimize the disturbances in the current wave before we supply to the load, see Figure 25.

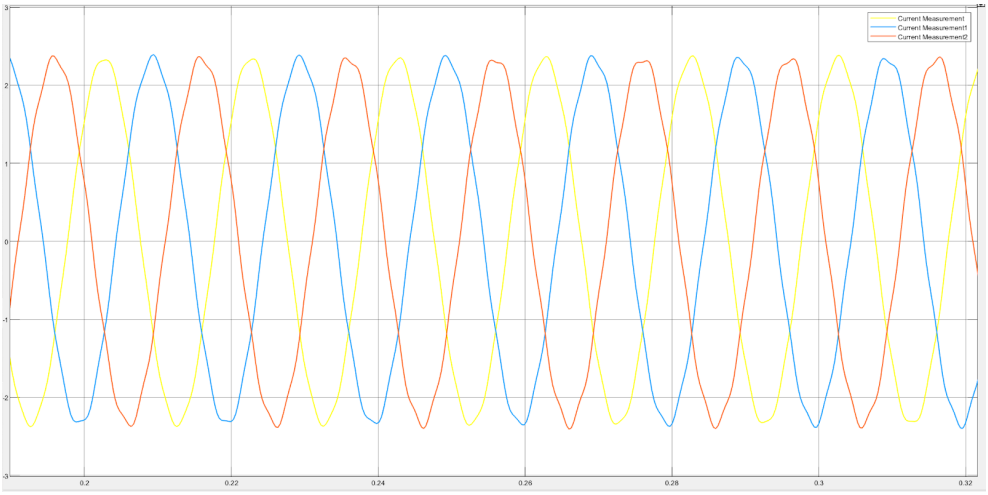

Figure 25: Current waves with harmonics

In the V2G mode when we induce the power back to the grid we need a pure sinusoidal waveform. However, the output from the converter is not a pure sine wave. LCL filter that we used before connecting to the grid smoothens the waveform into the pure sine wave, see Figure 26.

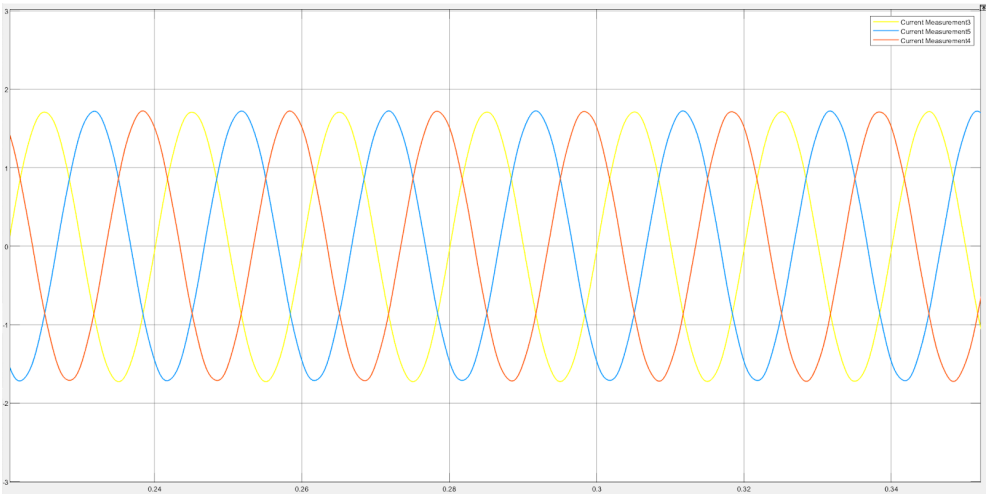

Figure 26: Current waveforms after the LCL filter

In the main V2G simulation, we connect the LCL filter between the 3-phase grid and the Voltage Source Converter VSC, as shown in Figure 27

3.2.4 AC-DC converter simulation

The voltage source convertor converts the AC to DC and also the DC to AC varying the switching sequence of the controlled switches. In this model, we have used the IGBTs as the switches, see Figure 28

We can also call the voltage source inverter as the front end converter. With the use of the control algorithm, we can generate the PWM for the switching sequence. So the

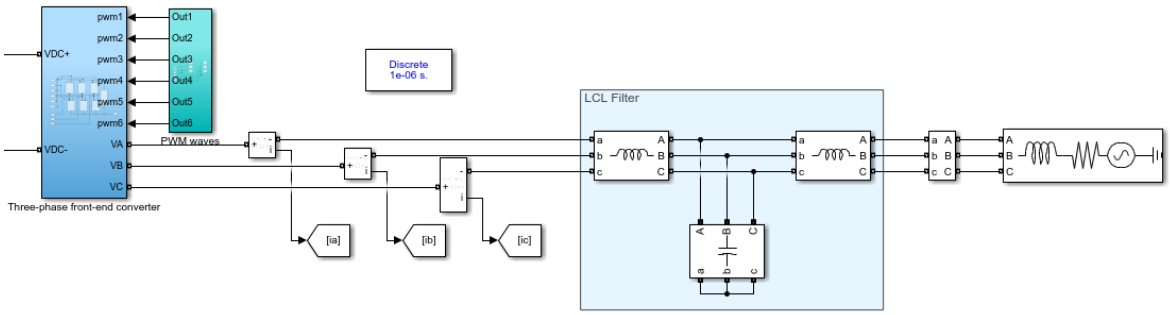

Figure 27: LCL filter in the V2G model

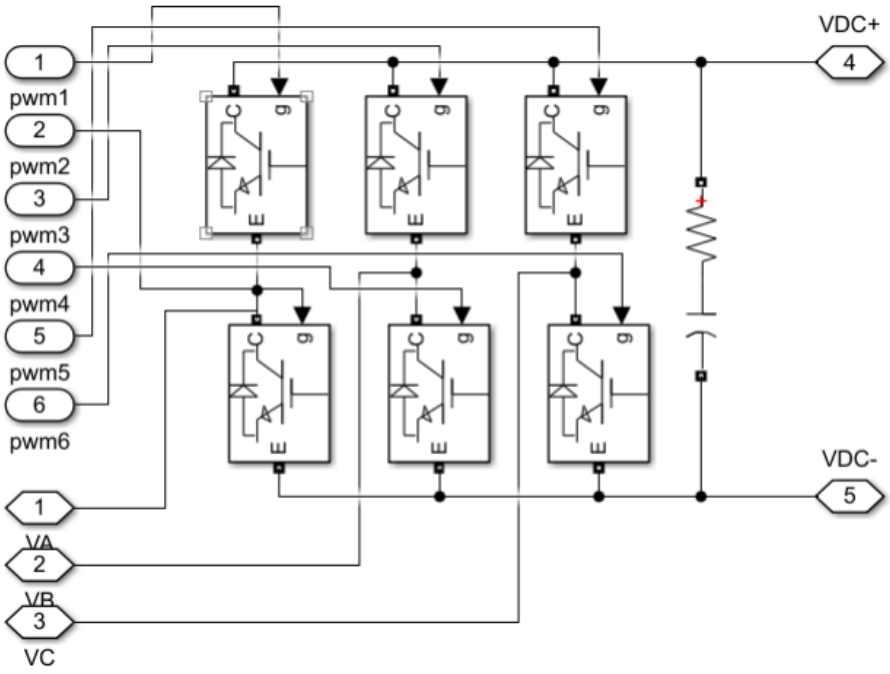

Figure 28: Voltage source convertor model

control starts from the voltage and current trasfermatiosn form *abc* to the *dq* frame using the Park and Clark transformations, as shown in Figure 29.

Then we model the voltage and current controllers where we give the voltage and current reference and bring the output close to the reference by reducing the error as much as possible using the PI control, see Figure 30.

The output signal from this control algorithm is used by to pulse generator to generate the PWM waves for switching the IGBTs, as shown in Figure 31.

As shown in Figure 32. By comparing the original signal with the carrier wave signal we can generate the required PWM for the VSC. The phase angle for the *abc* to *dq* transformation is generated from the PLL.

As a result of the switching sequence generated by the control algorithm the output voltage of the VSC is made constant setting close to the reference voltage with minimum possible error, see Figure 33.

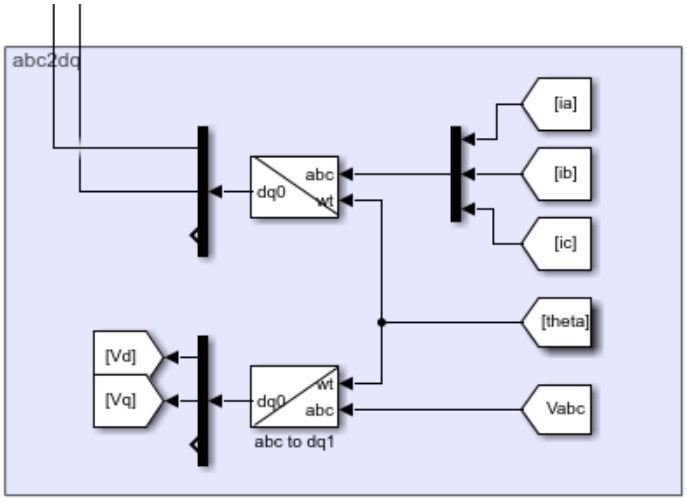

Figure 29: *abc* to *dq* transformation

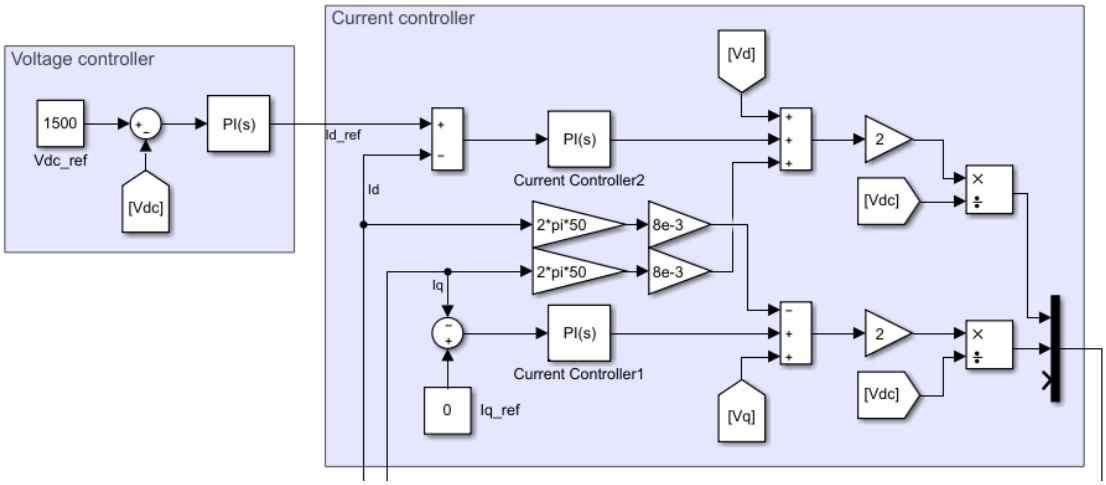

Figure 30: Voltage and current controllers

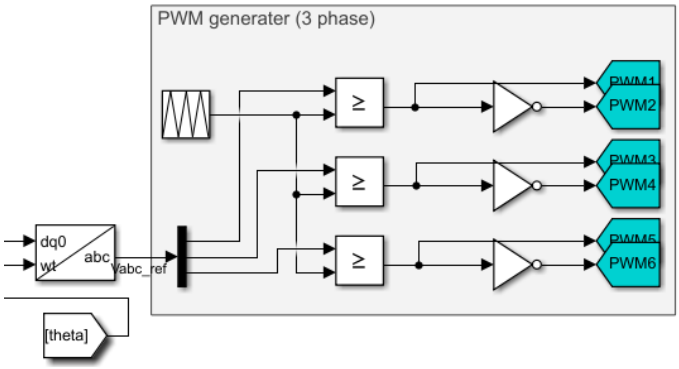

Figure 31: PWM generator

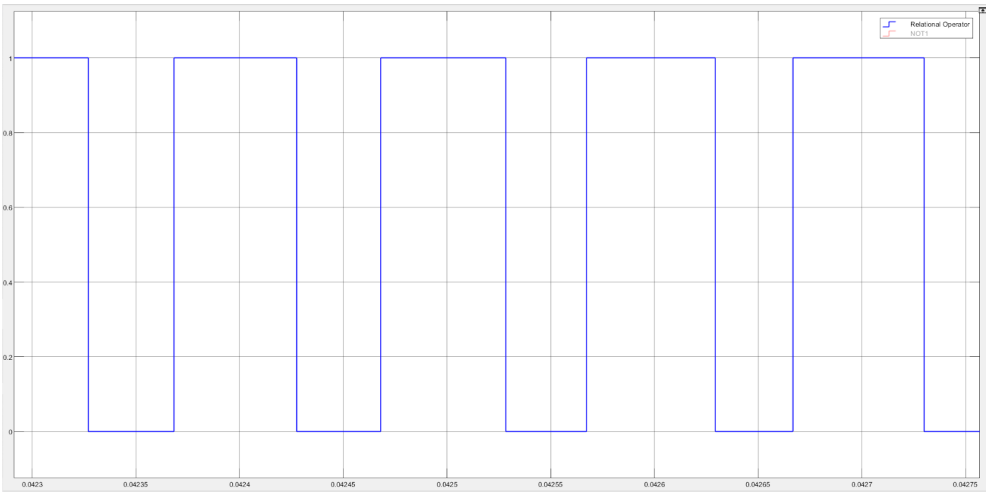

Figure 32: PWM signal for Leg 1

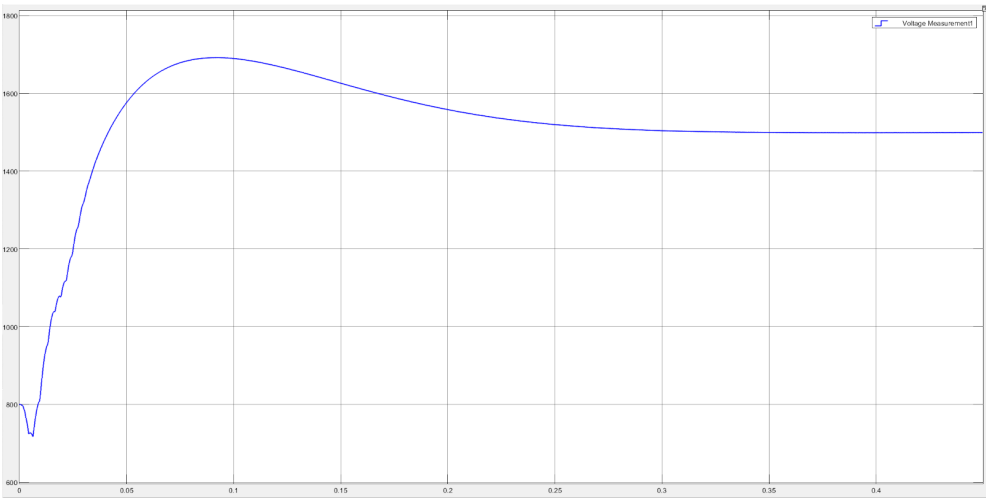

Figure 33: V_{dc} generated by the VSC

3.2.5 V2G and G2V simulation

The V2G model is integrated with the grid, DC-DC converter, AC/DC Converter, and output LCL filter, as Figure 34 shown.

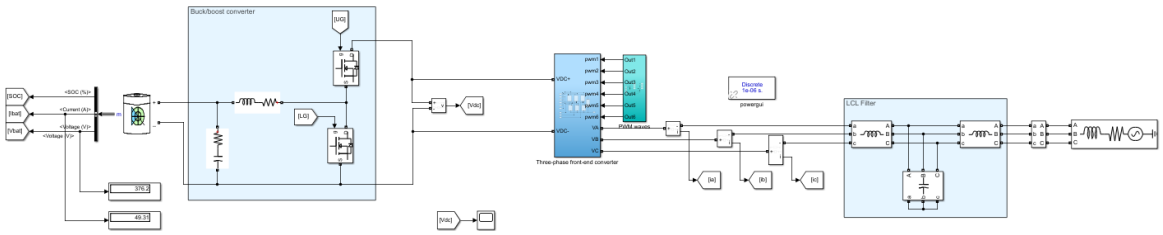

Figure 34: The simulation of the V2G system

The control algorithm is designed so that the power flow can be bidirectional. During the V2G mode, the vehicle battery will discharge to the gird or load (it can also be

motor in the vehicle). In the G2V mode, the power flow is from the grid to the vehicle. In this mode the vehicle charges.

In V2G mode using the PLL algorithm we can give necessary information about the phase angle of the voltage and current as well as frequency. So that we can use the information of the current control and voltage control algorithm to feed the power in synchronization with the grid. Before we feed the power to the grid as the output of VSC has the current harmonics, we use the LCL filter to smoothen it, see Figure 35 and 36.

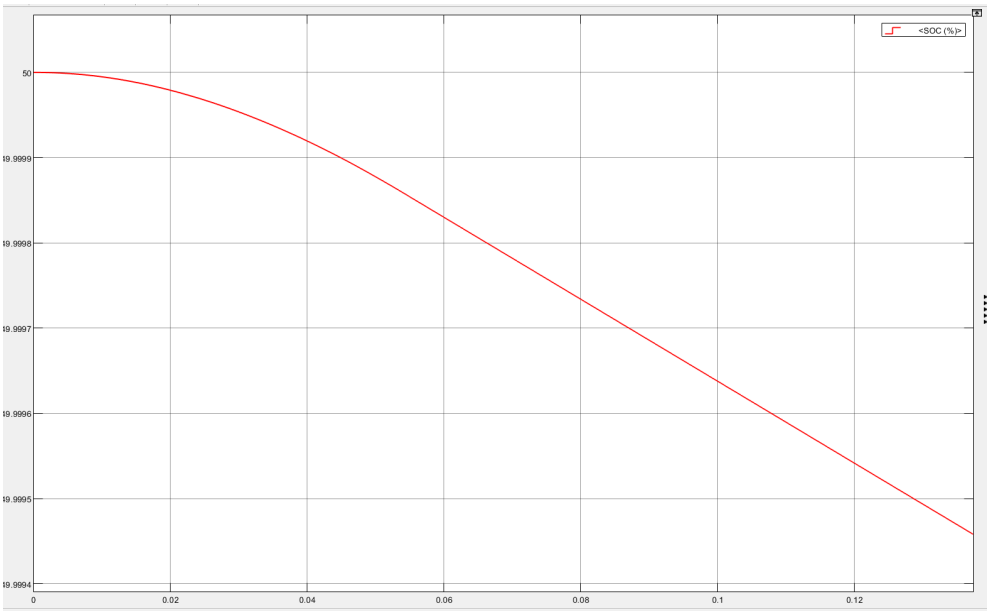

Figure 35: SOC during the V2G mode (Discharging mode)

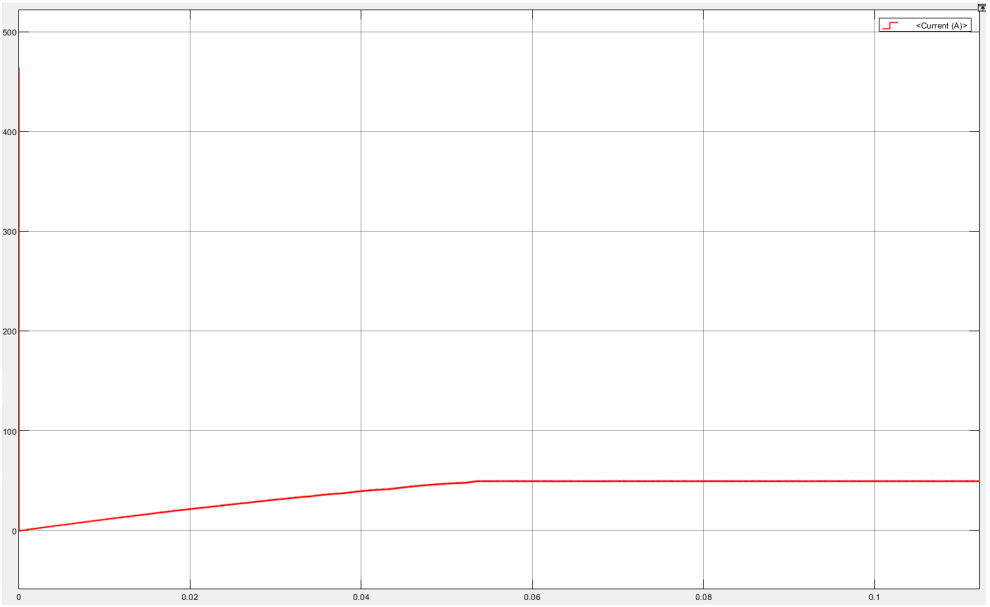

Figure 36: Current during the V2G mode (Discharging mode)

In Figure 37 we can see that the current is positive and this is the current discharged by the battery to charge the grid.

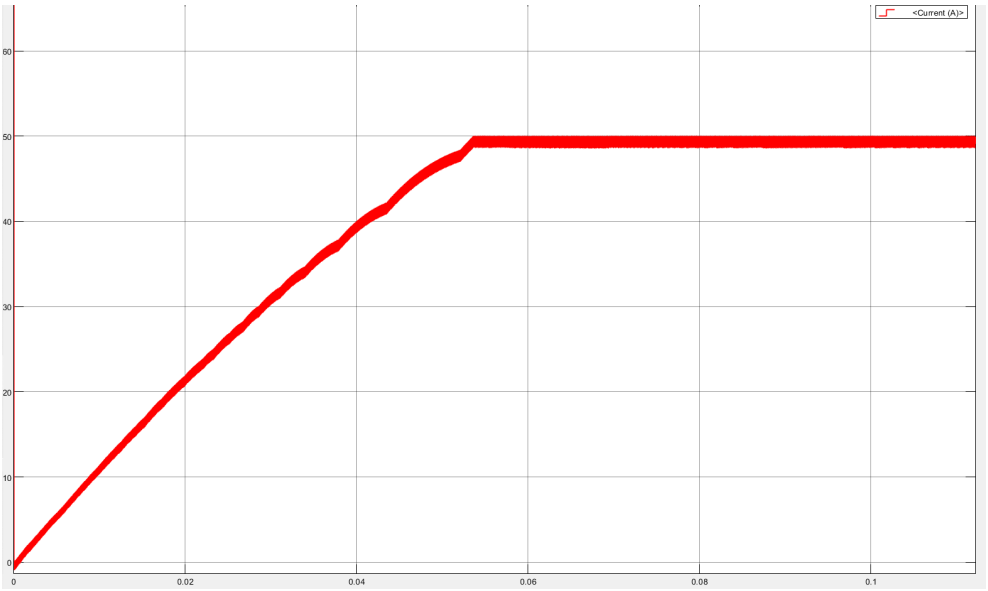

Figure 37: Chattering effect in current

Once the current reaches the set limit, the current keeps sliding between the saturation limits in order to main the constant output, as shown in Figure 38.

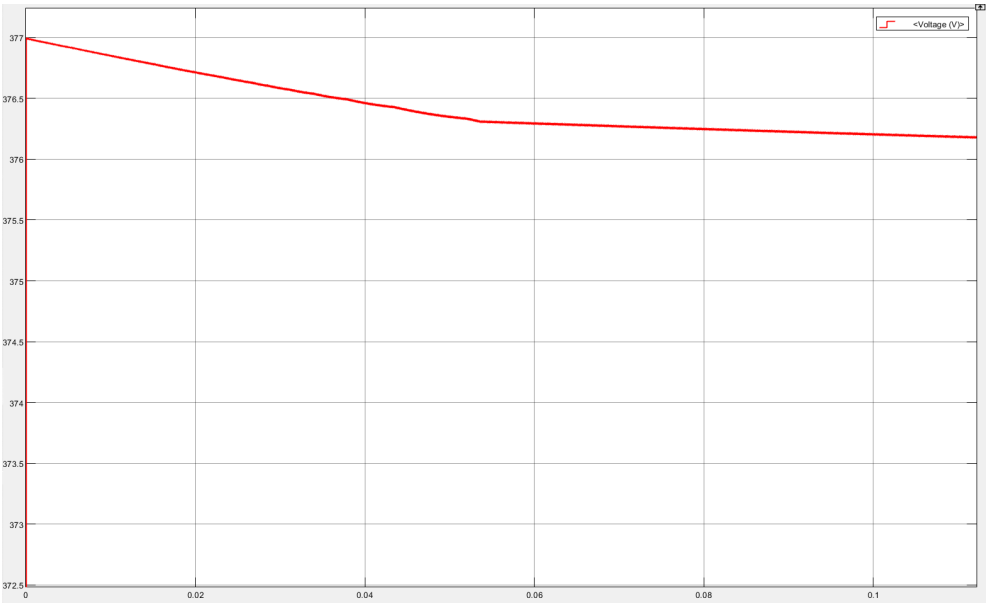

Figure 38: Battery voltage during the V2G mode (Discharging mode)

During the discharge of the Battery there is always a voltage drop at the terminal ends. So here the voltage keeps dropping as per the battery manufacturing profile. However, we have set the over-discharge and overcharge limits for the battery for its safe operation.

In V2G mode the converter works as a charger, the power is drawn from the grid to charge the vehicle battery, as shown in Figure 39 In this mode also we keep the current contest, for the slow charging we use lower limits, and for the fast charging, we use higher limits.

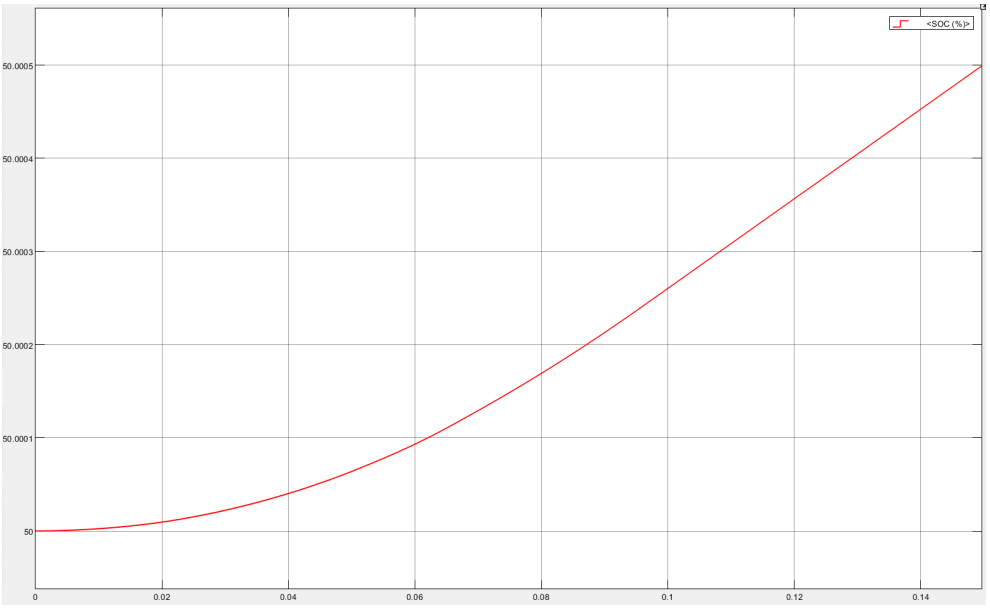

Figure 39: SOC during the G2V mode (Charging mode)

During the charging we see that the SOC is rising as the battery is charging by receiving the power from the grid, see Figure 40.

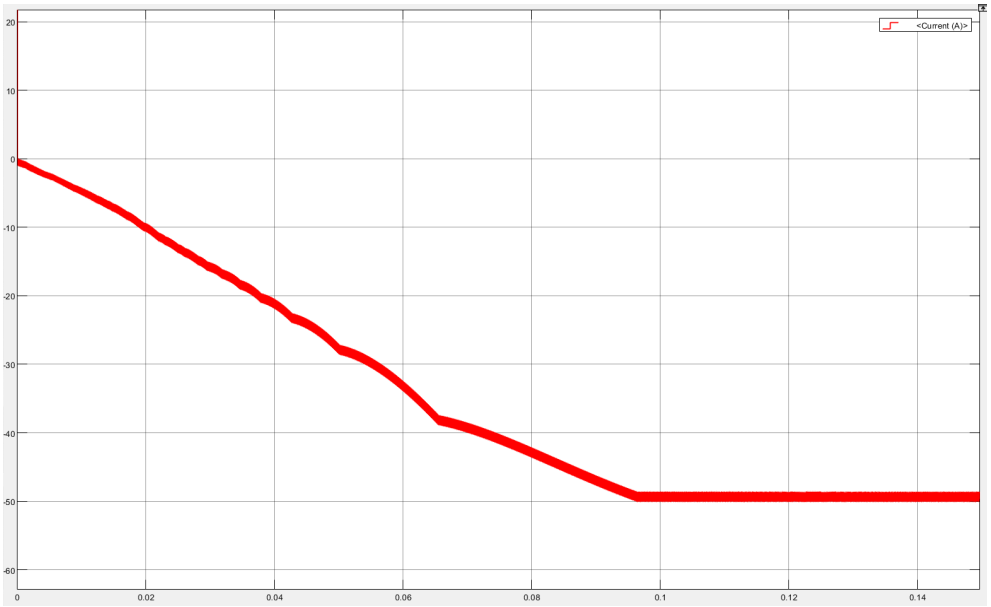

Figure 40: Current during the G2V mode (Charging mode)

In Figure 41, the current is fed to the battery to charge it. The current fed is made constant between the saturation limits to protect the battery from overheating due to faster chemical reactions.

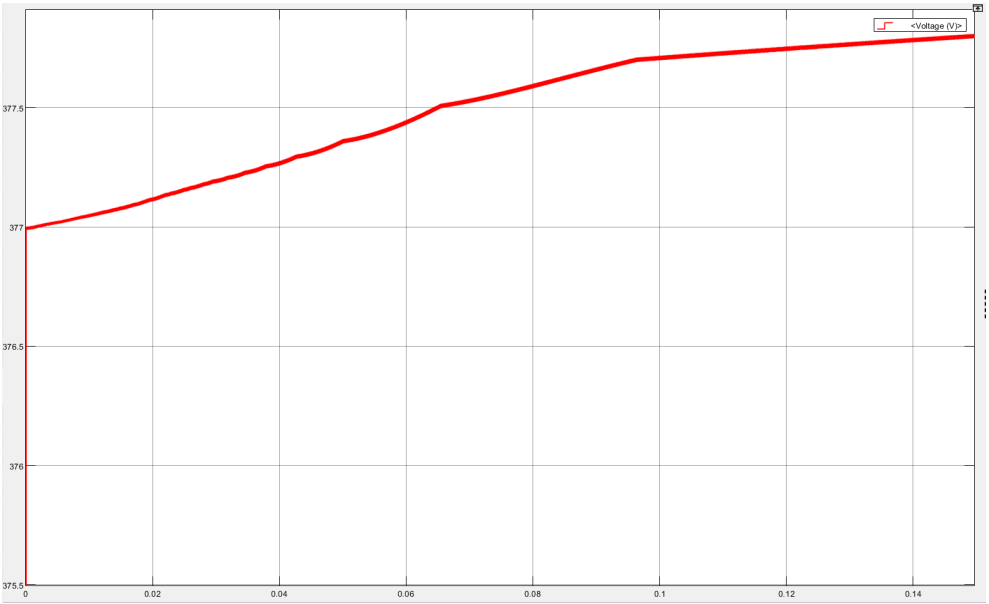

Figure 41: Voltage during the G2V mode (Charging mode)

During charging the voltage level of the battery increases. The terminal battery voltage keeps rising to its nominal and peak voltage values as the SOC come close to 100%.

References

[1] H. B. Sassi, F. Errahimi, N. Es-Sbai, and C. Alaoui, "A comparative study of ann and kalman filtering-based observer for soc estimation," in *IOP Conference Series: Earth and Environmental Science*, vol. 161, p. 012022, IOP Publishing, 2018.

[2] J. Han, X. Zhou, S. Lu, and P. Zhao, "A three-phase bidirectional grid-connected ac/dc converter for v2g applications," *Journal of Control Science and Engineering*, vol. 2020, 2020.

[3] C. M. Shepherd, "Design of primary and secondary cells: Ii. an equation describing battery discharge," *Journal of the Electrochemical Society*, vol. 112, no. 7, p. 657, 1965.

[4] O. Tremblay and L.-A. Dessaint, "Experimental validation of a battery dynamic model for ev applications," *World electric vehicle journal*, vol. 3, no. 2, pp. 289–298, 2009.

[5] A. Arancibia and K. Strunz, "Modeling of an electric vehicle charging station for fast dc charging," in *2012 IEEE International Electric Vehicle Conference*, pp. 1–6, IEEE, 2012.

[6] A. Arancibia, K. Strunz, and F. Mancilla-David, "A unified single-and three-phase control for grid connected electric vehicles," *IEEE transactions on smart grid*, vol. 4, no. 4, pp. 1780–1790, 2013.

[7] V.-L. Nguyen, T. Tran-Quoc, and S. Bacha, "Harmonic distortion mitigation for electric vehicle fast charging systems," in *2013 IEEE Grenoble Conference*, pp. 1–6, IEEE, 2013.

[8] M. Liserre, F. Blaabjerg, and S. Hansen, "Design and control of an lcl-filter-based three-phase active rectifier," *IEEE Transactions on industry applications*, vol. 41, no. 5, pp. 1281–1291, 2005.

[9] M.-Y. Park, M.-H. Chi, J.-H. Park, H.-G. Kim, T.-W. Chun, and E.-C. Nho, "Lcl-filter design for grid-connected pcs using total harmonic distortion and ripple attenuation factor," in *The 2010 International Power Electronics Conference-ECCE ASIA-*, pp. 1688–1694, IEEE, 2010.

[10] M. Liserre*, F. Blaabjerg, and A. Dell'Aquila, "Step-by-step design procedure for a grid-connected three-phase pwm voltage source converter," *International journal of electronics*, vol. 91, no. 8, pp. 445–460, 2004.

[11] A. K. Ziarani and M. Karimi-Ghartemani, "On the equivalence of three independently developed phase-locked loops," *IEEE transactions on automatic control*, vol. 50, no. 12, pp. 2021–2027, 2005.

[12] L. G. B. Rolim, D. R. da Costa, and M. Aredes, "Analysis and software implementation of a robust synchronizing pll circuit based on the pq theory," *IEEE Transactions on Industrial Electronics*, vol. 53, no. 6, pp. 1919–1926, 2006.

[13] M. Karimi-Ghartemani and M. R. Iravani, "A nonlinear adaptive filter for online signal analysis in power systems: Applications," *IEEE Transactions on Power Delivery*, vol. 17, no. 2, pp. 617–622, 2002.

[14] C. Wang, R. Xiong, H. He, X. Ding, and W. Shen, "Efficiency analysis of a bidirectional dc/dc converter in a hybrid energy storage system for plug-in hybrid electric vehicles," *Applied energy*, vol. 183, pp. 612–622, 2016.

[15] J. Siva Prasad, T. Bhavsar, R. Ghosh, and G. Narayanan, "Vector control of three-phase ac/dc front-end converter," *Sadhana*, vol. 33, no. 5, pp. 591–613, 2008.

[16] S.-K. Chung, "Phase-locked loop for grid-connected three-phase power conversion systems," *IEE Proceedings-Electric Power Applications*, vol. 147, no. 3, pp. 213–219, 2000.

[17] P. Rodríguez, J. Pou, J. Bergas, J. I. Candela, R. P. Burgos, and D. Boroyevich, "Decoupled double synchronous reference frame pll for power converters control," *IEEE Transactions on Power Electronics*, vol. 22, no. 2, pp. 584–592, 2007.

[18] E. Robles, S. Ceballos, J. Pou, J. L. Martin, J. Zaragoza, and P. Ibanez, "Variable-frequency grid-sequence detector based on a quasi-ideal low-pass filter stage and a phase-locked loop," *IEEE transactions on power electronics*, vol. 25, no. 10, pp. 2552–2563, 2010.

[19] EVSpecifications, "2021 tesla model x performance." https://www.evspecifications.com/en/model/7aaf10c.

[20] K. M. Tan, V. K. Ramachandaramurthy, and J. Y. Yong, "Bidirectional battery charger for electric vehicle," in *2014 IEEE Innovative Smart Grid Technologies-Asia (ISGT ASIA)*, pp. 406–411, IEEE, 2014.